Quasi-two-dimensional vortex matter in the ThH$_{10}$ superhydride

Andrey V. Sadakov [1] Vladimir A. Vlasenko [1] Dmitrii V. Semenok [2,*] Di Zhou [2,†]
Ivan A. Troyan [3] Alexey S. Usoltsev,[1] and Vladimir M. Pudalov [1,4]

[1]*P. N. Lebedev Physical Institute, Russian Academy of Sciences, Moscow 119991, Russia*
[2]*Center for High Pressure Science and Technology Advanced Research, Bldg. #8E, ZPark,*
10 Xibeiwang East Rd, Haidian District, Beijing, 100193, China
[3]*A. V. Shubnikov Institute of Crystallography of the Kurchatov Complex of Crystallography and*
Photonics (KKKiF), 59 Leninsky Prospekt, 119333 Moscow, Russia
[4]*National Research University Higher School of Economics, Moscow, 101000, Russia*

A comprehensive study of the vortex phases and vortex dynamics is presented for a recently discovered high-temperature superconductor ThH$_{10}$ with $T_C = 153$ K at 170 GPa. The obtained results strongly suggest a quasi-two-dimensional (2D) character of the vortex-glass phase transition in ThH$_{10}$. The activation energy yields a logarithmic dependence $U_0 \propto \ln(H)$ on magnetic field in a low-field region and a power-law dependence $U_0 \sim H^{-1}$ in a high-field region, signaling a crossover from 2D regime to three-dimensional collective pinning regime, respectively. Additionally, a pinning force-field dependence showcases dominance of surface-type pinning in the vicinity of T_C. Thermal activation energy (U_0), derived within thermally activated flux-flow theory, takes very high values above 2×10^5 K together with the Ginzburg number $Gi = 0.039$–0.085, which is lower only than those of BiSrCaCuO cuprates and 10–3–8 family of iron-based superconductor. This indicates the enormous role of thermal fluctuations in the dynamics of the vortex lattice of superhydrides, the physics of which is similar to the physics of iron-based and copper-based high-temperature superconductors.

I. INTRODUCTION

The discovery of superconductivity at 203 K in the sulfur hydride H$_3$S [1], anticipated on the basis of theoretical calculations [2,3], has stimulated great interest among the condensed-matter physics community. A tremendous amount of work was carried out, both theoretical [4–6] and experimental, leading to the emergence of a novel class of high-temperature superconductors (HTSCs)—metal superhydrides [4]. This new class of superconductors consists of several different structural types (Fig. 1): face-centered-cubic decahydrides: LaH$_{10}$ [7,8], ThH$_{10}$ [9], and CeH$_{10}$ [10]; cubic body-centered hexahydrides: YH$_6$ [11,12], CaH$_6$ [13], and EuH$_6$ [14]; hexagonal nonahydrides YH$_9$ [12], CeH$_9$ [10,15], ThH$_9$ [9], tetragonal LaH$_4$ [16–18], YH$_4$ [19], and A15-type polyhydrides, including La$_4$H$_{23}$ [20,21], Lu$_4$H$_{23}$ [22], and Y$_4$H$_{23}$ [23]. These structural classes of binary hydrides also cover the structures of ternary polyhydrides in cases where two metal atoms can replace each other's positions. Most of the mentioned hydrides and their crystal structures were first found as a result of theoretical studies long before their experimental discovery [24–27].

Superconductivity in hydrides emerges under extreme pressures, which can be achieved statically only in diamond-anvil cells (DACs). Unlike two other major families of

HTSCs—cuprates and iron-based superconductors (IBSCs), which were thoroughly investigated in the past by all available methods—the superhydrides are the least explored class of superconductors due to physically limited access to the high-pressure zone between two diamond anvils. Amongst the most significant experimental results firmly established for superhydrides are the observation of isotope effect, and magnetic(nonmagnetic) impurity scattering effect on the critical temperature (T_C). Still, much more effort is required to get reliable results on diamagnetic response [28,29], flux trapping [30], and resistive transitions in extreme magnetic fields [31]. Most recently, the experiments on self-field critical current allowed to tackle not only the energy gap value, but also estimate the London penetration depth in cubic SnH$_4$ [32]. However, until now there are very few works that studied the main properties of the mixed state in hydride superconductors. The mixed state governs properties of any type-II superconductor in magnetic fields $H > H_{C1}$. Studying the mixed state and the vortex matter in superhydrides is essential for further understanding of the physics behind the high-pressure superconductors, as well as for possible future applications of hydrides.

For cuprates and iron-based superconductors, it is firmly established that the ability to conduct current in magnetic fields without resistance in the vicinity of T_C mostly depends on the thermal fluctuations. In some cases, zero resistivity in the presence of weak magnetic fields can be achieved only at very low temperatures, because of the impact of thermal fluctuations. Generally, in layered HTSC the following
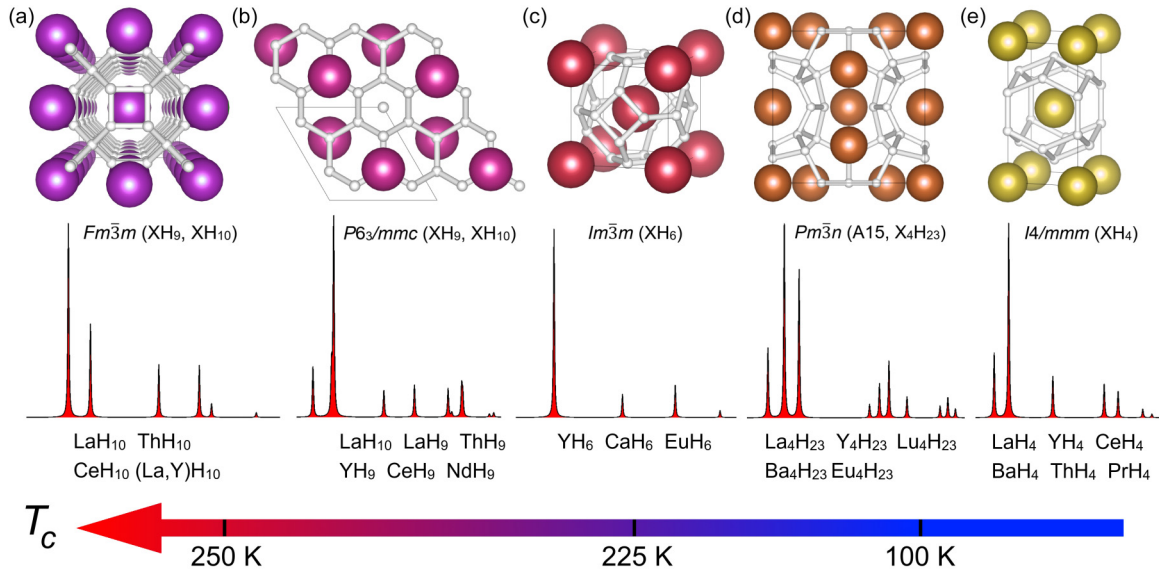

FIG. 1. Main structural classes of superconducting metal polyhydrides with examples of their lattice structure and x-ray diffraction signatures (a) fcc cubic deca- and nonahydrides with the highest known T_C values; (b) hexagonal nona- and decahydrides; (c) bcc cubic hexahydrides which also incorporate H_3S. (d) A15 class of cubic superhydrides, and (e) tetragonal superhydrides characterized by low stabilization pressure, but also by relatively low critical temperatures $T_C \approx 70$–100 K.

factors drastically increase the effect of fluctuations: high critical temperatures, short coherence length ξ, large penetration depth λ_L, and high anisotropy parameter γ. In superhydrides, ξ is short whereas λ_L is large, the critical temperatures are even higher, but the anisotropy ratio seem to be about unity due to highly symmetric structure similar to conventional low-temperature superconductors. In view of the above, it is therefore interesting to study how the increase in critical temperatures up to twice as much as in cuprates and 4–5 times as much as in IBSC alongside the isotropic nature of superhydrides will affect the vortex matter.

Recently, the vortex glass-liquid transitions in $Im\bar{3}m$-YH_6 with $T_C = 215$ K were studied, and it was shown that vortex motion in liquid phase is governed by thermal fluctuations, in a rather narrow ($\sim$1.5–2 K) region, but with very high activation barriers. This result seems to distinguish the yttrium superhydride YH_6 from other HTSCs in the vortex-matter physics. In order to check the generality of this result, we have chosen for study another member of the hydrogen-rich HTSC family, thorium decahydride, ThH_{10}, which has different critical parameters—lower critical temperature, larger coherence length, and larger penetration depth.

II. EXPERIMENTAL DETAILS AND SYNTHESIS OF ThH_{10}

Superconducting sample of $Fm\bar{3}m$-ThH_{10} was synthesized in a DAC by a pulsed Nd:yttrium aluminum garnet infrared laser (1.064 μm) heating of about 2-μm-thick thorium piece loaded in ammonia borane (NH_3BH_3) medium that plays the role of a source of hydrogen. Laser heating by 4–6 pulses, with a duration of each pulse about 300 ms, was performed under pressure of about 170 GPa. The diameter of the diamond anvils was 280 μm beveled at an angle of 8.5° to a culet of 50 μm. We used a composite insulating gasket made of CaF_2(epoxy) and a nonmagnetic steel. Additional details of

the synthesis, structural x-ray-diffraction studies, and characterization of the sample were published in Ref. [9].

Measurements of current-voltage characteristics and electrical resistance were performed with a combination of a Keithley 6221 dc current source and a Keithley 2182a nanovoltmeter (see Supplemental Material [33]), with a standard four-probe technique in the van der Pauw scheme. The Cernox temperature sensor was fixed directly on a diamond-anvil seat very close to the sample with a thermoconductive paste in order to correctly measure temperature of the sample. Experiments in magnetic fields were performed with the Cryogenic CFMS-16 system.

III. RESULTS AND DISCUSSION

A. Vortex glass and linear resistivity in ThH_{10}

According to the vortex-glass theory proposed by Fisher *et al.* [34,35] for type-II superconductors, the analysis of the linear current-voltage characteristics ($V \propto I$) in a low-current mode and corresponding temperature dependencies of the (linear) resistivity in magnetic fields may reveal the presence of a vortex glass. In the vicinity of the vortex-glass transition temperature T_g, the vortex matter in type-II superconductors with quenched disorder undergoes a second-order phase transition. This phase transition is characterized by the vortex-correlation length ξ_g and vortex-relaxation time τ_g of the fluctuations of the glassy-order parameter, and they both diverge at T_g. The correlation length diverges as $\xi_g \propto 1-T/T_g|^{-\nu}$, and the relaxation time diverges as $\tau_g \propto (\xi_g)^z \propto |1-T/T_g|^{-z\nu}$, where ν is the static exponent and z is the dynamic exponent. Then, linear resistivity vanishes following

$$\rho_{\text{lin}}(T) \propto |T - T_g|^s, \qquad (1)$$

where $s = \nu \times (z + 2 - d)$ and d is the sample dimensionality [34,35].

Moreover, current-voltage characteristics follow a scaling law, in which I-V isotherms below T_g and above T_g collapse into two distinct scaling curves in coordinates V_{scale} versus I_{scale}:

$$V_{scale} = (V/I) \times |1 - T/T_g|^{-\nu(z+2-d)};$$
$$I_{scale} = (I/T) \times |1 - T/T_g|^{-\nu(d-1)}. \qquad (2)$$

Fisher *et al.* also predicted that in 2D superconductors the vortex-glass phase transition can exist only at $T_g = 0$ K [36]. This was shown experimentally on 1.6-nm-thick Y-123 film [37] and on highly anisotropic Tl-2212 crystals with very weak coupling between superconducting layers [38]. However, for systems with lesser anisotropy 3D scaling procedures may give unphysically large value of z and very small value of ν [38]. Yamasaki *et al.* [39] proposed a model where vortex-glass correlation length in one dimension ($\xi_g^2 = \xi_\perp \xi_\parallel$) did not scale $\propto |T - T_g|$ for some reason, and demonstrated so-called quasi-2D behavior with $d = 2$. Later, it was shown by Sefrioui *et al.* [40] that in cuprates the situation depended on the system anisotropy, and the dimensionality of the vortex structure gradually went from 3D behavior (for low anisotropy) through quasi-2D behavior (for intermediate anisotropy) to pure 2D behavior (for high anisotropy).

Furthermore, in subsequent years, it was shown that the theory of quasi-two-dimensional vortex glass was applicable not only to highly anisotropic cuprates, but also to less anisotropic superconductors such as FeSe [41], MgB_2 [42], and even to isotropic superconductors such as thin films of TiO [43]. And if in cuprates, the quasi-two-dimensional behavior can be explained by the fact that the correlation along the direction of the magnetic field is broken due to the weak coupling between the superconducting planes. Then, in more isotropic films, it is most reasonable to associate the violation of correlation with the fact that the correlation length becomes comparable in order of magnitude to the thickness of the superconducting film.

1. Linear resistivity measurements

We start with investigation of the linear resistivity. Figure 2(a) shows temperature dependence of resistivity of ThH$_{10}$ sample, measured across the superconducting transition, at 170 ± 5 GPa in various magnetic fields up to 7 T. One can see that in zero magnetic field the sample experiences a superconducting transition at about $T_C = 153$ K (ρ_{50} criteria): below T_C the resistivity drops quickly to zero. The transition shifts to lower temperatures and slightly broadens as external magnetic field increases. The studied ThH$_{10}$ sample had the shape of a disk with ∼2-μm thickness and ∼ 20–25-μm diameter. In our measurements we used a current of ∼ 100 μA, and the resistivity was estimated according to the van der Pauw formula $\rho = R\pi t / \ln(2)$, where t is the sample thickness and R is the electrical resistance of sample.

In order to investigate the vortex-glass transition in ThH$_{10}$, we first analyzed the low-dissipation (linear) part of the resistive transitions. In Fig. 2(b), upper panel, we show $\ln(\rho)$ vs T curves for two magnetic field values. In the lower panel of this figure we show the inverse derivative $[d \ln(\rho)/dT]^{-1}$ vs T, recalculated for the same curves. One can see a linear region, showcasing the power-law dependence reminiscent of

Eq. (1) with T_g defined as an intercept with the T axis, and the slope of the line being $1/s$. The temperature where the inverse derivative deviates from linear behavior is marked as T^*, and it signifies an upper bound of the critical region, where the second-order vortex phase transition takes place.

A complete set of inverse derivatives for all magnetic fields is shown in Fig. 2(c). The values of the critical exponent for different fields vary approximately from 1.4 to 2.0 [see the inset of Fig. 2(c)]. These values are comparable to those obtained for cuprate HTSC, for example for heavily irradiated sample of YBCO in Ref. [44], where authors also obtained critical exponent ranging from $s = 1.2$ to 3 (for similar magnetic fields). According to the modified vortex-glass model, suggested by Andersson *et al.* [45,46], normalized linear resistivity in various magnetic fields in the critical region should scale into one universal curve in coordinates ρ/ρ_n vs $T_{scale} = [T(T_C - T_g)/T_g(T_C - T) - 1]$, where ρ_n is a resistivity in the normal state near superconducting transition. As can be seen in Fig. 2(d), the resistivity transitions in fields between 0.5 and 7 T scale into one curve with the critical exponent $s = 1.3 \pm 0.4$. Excellent agreement with the Andersson model for ThH$_{10}$ indicates the applicability of vortex-dynamics concepts to the hydride superconductors ThH$_{10}$ at ultrahigh pressures.

B. Temperature- and field-dependent I-V characteristics

It is worth noting that even though power-law behavior and scaling law of linear resistivity give significant evidence for the existence of the phase transition from vortex-liquid to -glass state, the most crucial and well-established proof for vortex-glass (VG) model is the scaling of current-voltage (I-V) characteristics. To explore this, we performed two sets of I-V experiments. In the first, a more traditional set, we stabilized magnetic field, and then measured I-V curves at different temperatures (T set). In the second experiment we stabilized temperature and measured I-V curves in different magnetic fields (H set).

The inset of Fig. 3(a) depicts a set of current-voltage characteristics of ThH$_{10}$ in a double-logarithmic scale for a magnetic field $H = 2$ T in the temperature range from 139 to 146 K. T_g can be approximately estimated from these log(I)-log(V) isotherms as the temperature at which the curvature changes from upturn to downturn with decreasing temperature. The "$T = T_g$" curve is represented by a dashed line. Then, we applied universal scaling for all I-V curves in coordinates of Eq. (2). As was found in the previous section, the linear resistivity data give rather small values of critical exponent $s = 1.3 \pm 0.4$ [from the universal scaling; see Fig. 2(d)] and 1.4–2.0 [from the inverse derivative data, Fig. 2(c)]. Such small values are usually inherent in a quasi-two-dimensional (quasi-2D) VG case [35], leading us to start scaling with parameter $d = 2$ in Eq. (2). As one can see [main panel of Fig. 3(a)], all ten I-V curves for $d = 2$ collapse into two distinct branches for $T < T_g$ and $T > T_g$. The dashed line corresponds to a power-law dependence $V \propto I^{(z+1)/(d-1)}$ for the $T = T_g$ case. From this scaling we obtain the static and dynamic exponents: $\nu = 1.90$ and $z = 0.41$. The vortex-glass transition temperature for $H = 2$ T was found to be 144.7 K, which is very close to T_g obtained from resistivity data.
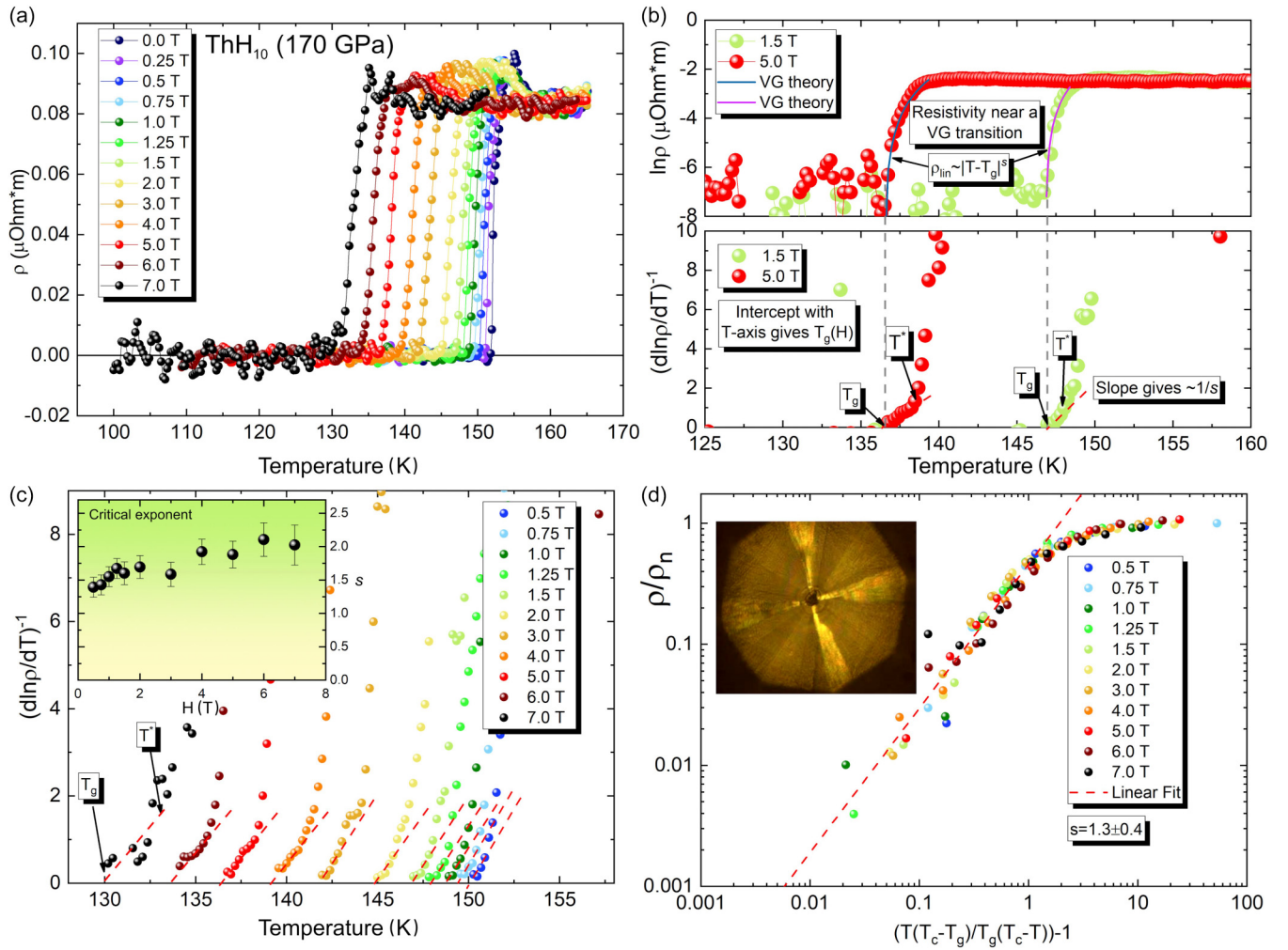
FIG. 2. Resistive transitions in thorium hydride ThH_{10} at 170 GPa. (a) In magnetic fields from 0 to 7 T (linear scale). (b) Interpolation of temperature dependence of resistivity and its temperature derivative (logarithmic scale) using vortex glass (VG) model $\rho_{lin}(T) \propto |T - T_g|^s$ at 1.5 and 5 T. Corresponding extrapolation of the model to the intersection with the temperature axis (T axis) gives us the melting temperature (T_g) of the vortex glass in ThH_{10}. (c) Full set of the inverse temperature derivatives of $\ln(\rho)$ for applied magnetic fields from 0.5 to 7 T. Red dotted lines correspond to linear interpolation near T_g. (d) Universal scaling of relative resistivity vs rational function of T_C, T_g, and T in magnetic fields of 0.5–7 T. Inset: photo of the ThH_{10} sample with electrical leads. A detailed description of the measurements is given in the Supplemental Material.

The second set of current-voltage characteristics, which was measured at fixed temperature and in different magnetic fields (H set) is shown in Fig. 3(b) (inset) in double-logarithmic scale. Here, we can estimate the vortex-glass transition field H_g, at which I-V dependences change their curvature (marked by dashed line). The main panel of Fig. 3(b) shows that the I-V curves for $d = 2$ are collapsing into two distinct brunches for $H < H_g$ and $H > H_g$. The dashed line corresponds to a power-law dependence $V \propto I^{(z+1)/(d-1)}$, for the $H = H_g$ case. Resulting scaling parameters are $\nu = 2.15$ and $z = 0.53$. The vortex-glass transition field for $T = 148.4$ K was found to be $H_g = 1.15$ T. The critical exponent $s = \nu(z + 2 - d)$ for two sets of I-V curves are 0.78 and 1.14, which is rather close to the value of $s = 1.3$ obtained from linear resistivity scaling [Fig. 2(d)] and $s = 1.4$–1.5 obtained from inverse derivatives in low fields [Fig. 2(c)].

The scaling parameter ν (static exponent), determined from this analysis, ranges from 1.90 to 2.15 that is consistent with

the bulk vortex-glass models (ν varying from 1 to 2) [35]. At the same time, the dynamic exponent z appears to lie between 0.41 and 0.53, which is much lower than commonly reported values, falling in the range from 4 to 7. We note, however, that similar small values of z are typical for several cases, reported in quasi-2D systems: FeSe thin film [41] (z varying from 0.43 to 0.56), $Bi_2Sr_2Ca_2Cu_3O_{10+\delta}$ submi-crobridges [47] (z varying from 0.38 to 0.39), $YBa_2Cu_3O_x$ thin films [48], and bulk $FeSe_{1-x}S_x$-layered system [49] ($z = 0.82$ for 6 T).

In order to double check the above quasi-2D scaling we applied the same critical scaling procedure with $d = 3$. The results of the scaling are as follows: $\nu = 0.88$ and $z = 1.74$ (see Supplemental Material, Fig. S1). As one can see, the scaling results for $d = 3$ are much less consistent with the linear resistivity data [$s = \nu(z + 2 - d) = 0.6$ for T set] and are inconsistent with generally expected values of the critical exponents for 3D case. Usually, in three-dimensional case, ν
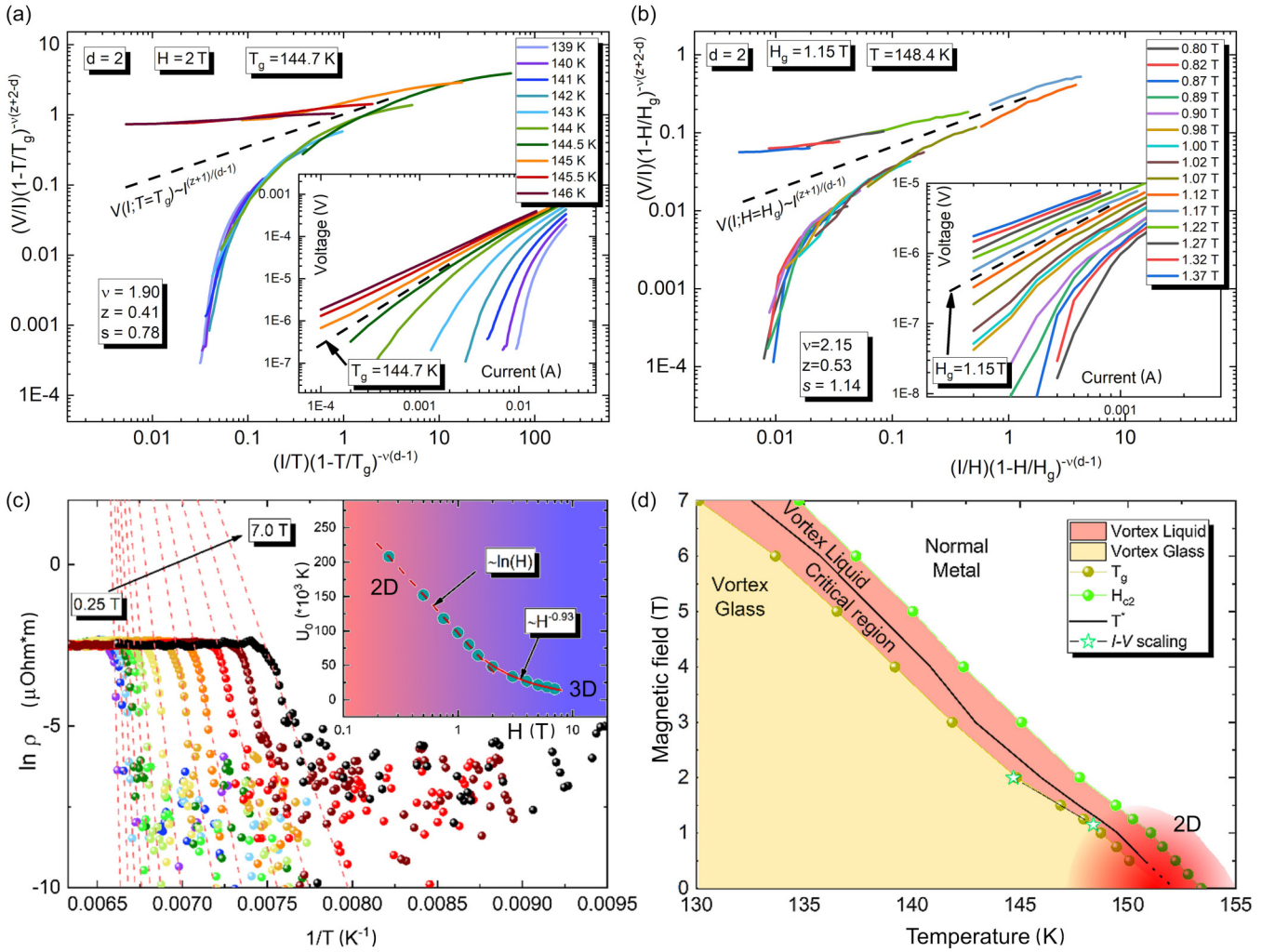
FIG. 3. Quasi-two-dimensional dynamics of the vortex lattice in ThH$_{10}$. (a) Current-voltage characteristics of ThH$_{10}$ in the double-logarithmic scale of Eq. (2) for a magnetic field $H = 2$ T in the temperature range from 139 to 146 K (T set). Inset: *I-V* characteristics in a double-logarithmic scale. (b) Current-voltage characteristics of ThH$_{10}$ in the double-logarithmic scale at 148.4 K in the range of magnetic fields from 0.8 to 1.37 T (H set). The scaling for H set of *I-V* curves is performed in the same manner as the one for T set with isotherms, but in this case, the scaling coordinates [Eq. (2)] will have temperature-dependent term T/T_g substituted by the field-dependent term H/H_g in accordance with similar vortex-glass investigations [50,51]. (c) Arrhenius plot $\ln(\rho)$ vs $1/T$, where ρ is resistivity of the sample with assumed thickness of 2 μm. The dashed red lines are fitting results from the Arrhenius relation. Inset: field dependence of apparent activation energy $U_0 = -d(\ln\rho)/d(1/T)$ (y axis) and magnetic field (x axis) in semilogarithmic scale. (d) Vortex phase diagram of ThH$_{10}$ at 170 GPa.

varies from 1 to 2, *z* belongs to the 4–7 interval, and *s* lies between 2.7 and 9 [35].

Summarizing the results of this section, we can state that according to the linear resistivity scaling, inverse derivative data and universal critical scaling for two sets of *I-V* curves, the vortex-glass state emerges in the ThH$_{10}$ superconductor as a possible quasi-2D-state, at least in fields up to 2 T. The obtained values of the critical exponents (*s*, *v*, and *z*) are similar to those in several preceding experiments where quasi-2D vortex glass was studied in highly anisotropic HTSCs [47], and also in systems with rather low anisotropy (like FeSe and FeSe$_{1-x}$S$_x$ [47]). The low dimensionality of vortex system occurs in superconductor when vortex correlation length becomes comparable with either distance between weakly coupled superconducting planes (like in most cuprates and

some iron-based HTSCs), or one of sample dimensions, or distance between planar defects, such as grain boundaries, with absent or suppressed superconductivity. We believe both latter scenarios are possible for polycrystalline ThH$_{10}$ sample. The most logical proof that the correlation length becomes comparable to the thickness of the sample would be a series of experiments with different crystal thicknesses, which was done for cuprates, for example. Unfortunately, at the current stage of experimental capabilities in superhydride physics, this is almost impossible to do, because the thickness of the sample is quite strictly tied to the thermodynamic stability pressure of the superconducting phase. It should be also noted that the discrepancy of the scaling parameters even in the quasi-2D approximation may also indicate more complicated vortex dynamics in ThH$_{10}$, which is beyond the current

theoretical models. In order to verify this assumption, a wide discussion in terms of theoretical description and experimentation results is required.

We also performed a detailed investigation of pinning force and critical current field dependences, which can give us information of the type of defects and geometry of pinning centers. The existence of the planar defects is very difficult to establish without scanning technique, like transmission electron microscope (TEM) [52]. However, it is possible to determine the geometry of defects in a superconductor from studying the field dependence of the pinning force. According to flux-pinning theory, developed by Dew-Hughes [53], the pinning force $F_p = I_c * H$ has a strictly defined functional dependence for each of the individual types of defect geometry: volume, surface, or pointlike. The details of the pinning force investigation are presented in Supplemental Material, Fig. S2. The results show, that in the vicinity of T_C pinning force follows the functional dependence $F_p \propto h^{0.6}(1–h)^{2.1}$, with maximum at $h_{max} = 0.22$ ($h = H/H_{irr}$ is the reduced field, and H_{irr} is the irreversibility field). This dependence is in very good agreement with the one $F_p \propto h^{0.5}(1–h)^{2.0}$ (where $h_{max} = 0.2$) theoretically predicted for normal-core surfacelike pinning centers. Thus, our analysis of the pinning force indicates the presence of surface defects in the sample, which supports one of the two possible scenarios for the quasi-2D character of the vortex matter in ThH$_{10}$.

C. Vortex liquid and the thermally activated flux-flow theory

Above the melting line, the vortex glass undergoes a phase transition into the vortex-liquid state. Here, the dynamics of the system is regulated by the competing contributions of vortex motion, guided by thermal energy $k_B T$ and the effective pinning energy $U(T, H)$. If the pinning energy is smaller than the temperature, they can be neglected and then the system is in unpinned vortex-liquid state. However, if $U(T, H)$ is higher than the temperature, then energy barriers play vital role in vortex motion via thermally activated mechanism and the system is in the TAFF state. According to the thermally activated flux-flow (TAFF) theory [35,54], if the applied current is small enough then a temperature dependence of resistivity is defined as

$$\rho(T, H) = \rho_0 \exp[-U(T,H)/T], \quad (3)$$

where $U(T, H)$ is the activation energy, and prefactor ρ_0 is in general case dependent on both temperature and magnetic field. However, for the most of experimental studies in iron-based superconductors, cuprates, and conventional superconductors it is assumed that ρ_0 is temperature independent, and the activation energy is defined as $U(T,H) = U_0(H) \times (1–T/T_C)$. Here, U_0 is the apparent activation energy. With these two assumptions, natural logarithm of the linear electrical resistivity [Eq. (3)] is expressed as

$$\ln \rho(T, H) = \ln \rho_0 - [U_0(H)/T] + [U_0(H)/T_C]. \quad (4)$$

Equation (4) is known as the Arrhenius relation, and the plot in $\ln(\rho)$ vs $1/T$ coordinates will exhibit a linear behavior in the TAFF regime [49,55]. In Fig. 3(c), we present $\ln(\rho)$ vs $1/T$ plots for different magnetic fields from 0.25 to 7 T, in order to find the temperature region that satisfies the

Arrhenius relationship [Eq. (4)]. As Fig. 3 shows, for each magnetic field there is a distinct linear region marked by red dashed lines, following TAFF regime, and its slope gives us the activation energy $U_0(H)$. The magnetic field dependence $U_0(H)$ is presented in the inset of Fig. 3(c). As one can see, the flux-pinning activation energy shows two distinct regions in semilogarithmic scale. In one region, from 0.25 up to 1.5 T, it exhibits a logarithmic behavior $U_0(H) \propto -\ln(H)$, and at higher fields we see a crossover to $U_0(H) \propto 1/H$ behavior, thus suggesting different mechanism for activated vortex motion in these field regions. We estimated the flux-flow barriers $U_0(H) = 1.5–20 \times 10^4$ K to be very high (for $H = 2$ T), even higher than in YH$_6$ [56].

Usually the $U_0(H) \propto -\ln(H)$ behavior is observed in many 2D [57–59] and quasi-2D systems [60,61], in agreement with the results of the previous sections. There are several possible mechanisms which can be responsible for these particular field dependences of the activation energy. The first mechanism that leads to logarithmic behavior of pinning energy is the motion of thermally activated vortex-antivortex pairs, observed, for example, in highly anisotropic Bi-2212 cuprates [62], where interplanar coupling is particularly weak. It was proposed by Jensen *et al.* [63] that this type of vortex movement is associated with activation energy:

$$U_{V-V^a} = \frac{\phi_0^2 d}{4\pi \lambda_L(T)^2} \ln\left(\frac{a_0}{\xi(T)}\right), \quad (5)$$

where λ_L and ξ are the London penetration depth and coherence length, respectively, ϕ_0 is a flux quantum, d is the thickness of the superconductor, and $a_0 = (\phi_0/H)^{0.5}$ is the flux-line spacing. Equation (5) describes logarithmic decrease of the activation energy with magnetic field. However, we believe it is highly unlikely that vortex-antivortex case, which was only observed in very specific quasi-2D systems, is applicable for a polycrystalline hydride system like our ThH$_{10}$ sample.

The second mechanism that leads to logarithmic behavior of pinning energy is the nucleation of edge-dislocation pairs in the vortex system. Following Ref. [64], the energy required to unbind a small dislocation pair is finite and leads to an activation energy given by

$$U_{edge} = \frac{\phi_0^2 d}{16\pi \lambda_L(T)^2} \ln\left(\frac{a_0}{\xi(T)}\right), \quad (6)$$

which is very similar to Eq. (5) and leads to similar $U_0(H) \propto -\ln(H)$ dependence.

The next possible mechanism of dissipation is the vortex cutting and reconnection in the entangled vortex liquid, proposed in Ref. [65]. Entangled vortices can cut each other if the distance between them decreases below the average flux-line spacing a_0 and becomes comparable to the vortex core diameter ξ. The energy required for cutting (neglecting the energy due to the vortex elongation) is

$$U_{cut} = \frac{\phi_0^2 d}{32\pi^2 \lambda_L(T)^2} \ln\left(\frac{a_0}{\xi(T)}\right). \quad (7)$$

As one can see from Eqs. (5)–(7) the prefactors before logarithm (with slightly different numerical multipliers) are dependent on the superconductor thickness, d, and London

penetration depth. Following the steps in Ref. [61], we now estimate the correlation length ξ_g for our vortex system, using the experimental slope of activation energy $U \propto \ln(H)$ dependence, and London penetration depth obtained from self-field critical-current experiments in accordance with Refs. [66,67] and also Ref. [32] (for details, see Supplemental Material, Fig. S3). Resulting values of the correlation length ξ_g are 6.5 and 13 μm for Eqs. (6) and (7), respectively. Both correlation-length estimations exceed our sample thickness ($d \sim 2$ μm), validating the assumption of quasi-2D behavior of vortex liquid in ThH$_{10}$ in weak magnetic fields. However, within our investigations, we are unable to exclude any of the two possible mechanisms for thermally activated dissipation.

The power-law behavior of activation energy in higher fields $U \propto 1/H$ [as shown in the lower inset in Fig. 3(c)] starts at approximately 1.5 T and goes up to 7 T. The H^α dependence with $\alpha = -1$ behavior is rather typical for high-T_C cuprate superconductors [61,68], iron-based superconductors [69], and boride superconductors [70]. Such power law is associated with three-dimensional collective pinning regime [69,71,72]. In this regime, when magnetic fields are high enough, so that the intervortex interaction becomes significant, U_0 is controlled by collective pinning of the vortex bundles confined by a field-dependent correlation volume [73,74]. Thus, our results depict a crossover in the vortex activation energy from two-dimensional regime, controlled by either vortex-edge dislocations or vortex cutting, to three-dimensional regime, controlled by collective pinning of the vortex bundles.

Finally, based on the values of $H_{C2}(T)$, $T_g(H)$, $T^*(H)$, a detailed H-T vortex phase diagram is constructed in Fig. 3(d), reflecting all the experimental data and theoretical investigations of linear resistivity, universal I-V scaling, and thermally activated vortex motion. We were able to distinguish four different regions in the mixed state of $Fm\bar{3}m$-ThH$_{10}$ superconductor: (i) Vortex-glass region, displaced below the melting line $T_g(H)$; (ii) Critical region between $T_g(H)$ and $T^*(H)$ lines, where a gradual phase transition takes place; (iii) quasi-2D TAFF region above the $T^*(H)$ line in fields $H < 1.5$ T; and (iv) 3D collective-pinning region. Using $T_C = 153$ K, $H_{C2}(0) = 40$ T, and $\xi = 2.87$ nm, we estimated the Ginzburg number for ThH$_{10}$ as $Gi = 0.039$–0.085. Such large values are typical for cuprates [35] and iron-containing pnictides [75], indicating a direct analogy in the dynamics

of vortex matter between cuprate HTSC superconductors and thorium ThH$_{10}$ and yttrium YH$_6$ [56] superhydrides.

IV. CONCLUSIONS

To summarize, we have studied the complex vortex state in a ThH$_{10}$ high-temperature superconductor under 1.7-Mbar pressure. Our results suggest possible quasi-two-dimensional nature of the vortex-glass state, reminiscent of copper-based superconductors and some other systems. Within the framework of TAFF theory we established that vortex motion in liquid state is governed by strong thermal fluctuations. Thermal activation energy (U_0) and the Ginzburg number are very high in ThH$_{10}$: U_0 exceeds 2×10^5 K and $Gi = 0.039$–0.085, respectively. In terms of these parameters, the thorium hydride approaches the records of BiSrCaCuO system and Ca$_{10}$(Pt$_3$As$_8$)[(Fe$_{1-x}$Pt$_x$)$_2$As$_2$]$_5$ [76]. Magnetic field dependence of activation energy exhibits a crossover at field $H_{cr} = 1.5$ T from a quasi-2D logarithmic behavior $U_0 \propto \ln(H)$ to 3D power-law behavior $U_0 \propto 1/H$, apposite for collective-pinning regime. The analysis of low-dissipation region of linear resistivity in combination with universal scaling of current-voltage characteristics allows us to assert the existence of the vortex-glass state, its melting line $T_g(H)$, and critical region in accordance with the VG theory.

The raw data that support the findings of this study are available in the Supplemental Material of this and on the GitHub [79].

ACKNOWLEDGMENTS

[1] A. P. Drozdov, M. I. Eremets, I. A. Troyan, V. Ksenofontov, and S. I. Shylin, Conventional superconductivity at 203 kelvin at high pressures in the sulfur hydride system, Nature (London) **525**, 73 (2015).

[2] D. Duan, Y. Liu, F. Tian, D. Li, X. Huang, Z. Zhao, H.u Yu, B. Liu, W. Tian, and T. Cui, Pressure-induced metallization of dense (H$_2$S)$_2$H$_2$ with high-Tc superconductivity, Sci. Rep. **4**, 6968 (2014).

[3] Y. Li, J. Hao, H. Liu, Y. Li, and Y. Ma, The metallization and superconductivity of dense hydrogen sulfide, J. Chem. Phys. **140**, 174712 (2014).

[4] I. A. Troyan, D. V. Semenok, A. G. Ivanova, A. G. Kvashnin, D. Zhou, A. V. Sadakov, O. A. Sobolevsky, V. M. Pudalov, and

A. R. Oganov, High-temperature superconductivity in hydrides, Phys. Usp. **65**, 748 (2022).

[5] C. J. Pickard, I. Errea, and M. I. Eremets, Superconducting hydrides under pressure, Annu. Rev. Condens. Matter Phys. **11**, 57 (2020).

[6] B. Lilia *et al.*, The 2021 room-temperature superconductivity roadmap, J. Phys.: Condens. Matter **34**, 183002 (2022).

[7] A. P. Drozdov *et al.*, Superconductivity at 250 K in lanthanum hydride under high pressures, Nature (London) **569**, 528 (2019).

[8] I. A. Kruglov *et al.*, Superconductivity of LaH$_{10}$ and LaH$_{16}$ polyhydrides, Phys. Rev. B **101**, 024508 (2020).

[9] D. V. Semenok, A. G. Kvashnin, A. G. Ivanova, V. Svitlyk, V. Yu. Fominski, A. V. Sadakov, O. A. Sobolevskiy, V. M. Pudalov, I. A. Troyan, and A. R. Oganov, Superconductivity at 161 K in thorium hydride ThH_{10}: Synthesis and properties, Mater. Today **33**, 36 (2020).

[10] W. Chen, D. V. Semenok, X. Huang, H. Shu, X. Li, D. Duan, T. Cui, and A. R. Oganov, High-Temperature superconducting phases in cerium superhydride with a Tc up to 115 K below a pressure of 1 megabar, Phys. Rev. Lett. **127**, 117001 (2021).

[11] I. A. Troyan *et al.*, Anomalous high-temperature superconductivity in YH_6, Adv. Mater. **33**, 2006832 (2021).

[12] P. Kong *et al.*, Superconductivity up to 243 K in the yttrium-hydrogen system under high pressure, Nat. Commun. **12**, 5075 (2021).

[13] L. Ma *et al.*, High-Temperature superconducting phase in clathrate calcium hydride CaH_6 up to 215 K at a pressure of 172 GPa, Phys. Rev. Lett. **128**, 167001 (2022).

[14] L. Ma, M. Zhou, Y. Wang, S. Kawaguchi, Y. Ohishi, F. Peng, H. Liu, G. Liu, H. Wang, and Y. Ma, Experimental clathrate superhydrides EuH_6 and EuH_9 at extreme pressure conditions, Phys. Rev. Res. **3**, 043107 (2021).

[15] X. Li *et al.*, Polyhydride CeH_9 with an atomic-like hydrogen clathrate structure, Nat. Commun. **10**, 3461 (2019).

[16] D. Laniel *et al.*, High-pressure synthesis of seven lanthanum hydrides with a significant variability of hydrogen content, Nat. Commun. **13**, 6987 (2022).

[17] W. Chen, X. Huang, D. V. Semenok, S. Chen, D. Zhou, K. Zhang, A. R. Oganov, and T. Cui, Enhancement of superconducting critical temperature realized in La-Ce-H system at moderate pressures, Nat. Commun. **14**, 2660 (2023).

[18] J. Bi *et al.*, Stabilization of superconductive La-Y alloy superhydride with Tc above 90 K at megabar pressure, Mater. Today Phys. **28**, 100840 (2022).

[19] M. Shao, W. Chen, K. Zhang, X. Huang, and T. Cui, High-pressure synthesis of superconducting clathratelike YH_4, Phys. Rev. B **104**, 174509 (2021).

[20] J. Guo, D. Semenok, G. Shutov, D. Zhou, S. Chen, Y. Wang, K. Zhang, X. Wu, S. Luther, T. Helm, X. Huang, and T. Cui, Unusual metallic state in superconducting A15-type La_4H_{23}, Natl. Sci. Rev. nwae149 (2024).

[21] S. Cross, J. Buhot, A. Brooks, W. Thomas, A. Kleppe, O. Lord, and S. Friedemann, High-temperature superconductivity in La_4H_{23} below 100 GPa, Phys. Rev. B **109**, L020503 (2024).

[22] Z. Li *et al.*, Superconductivity above 70 K observed in lutetium polyhydrides, Sci. China: Phys. Mech. Astron. **66**, 267411 (2023).

[23] E. Siska *et al.*, Ultra-fast yttrium hydride chemistry at high pressures via non-equilibrium states induced by x-ray free electron laser, arXiv:2307.11293.

[24] H. Wang, J. S. Tse, K. Tanaka, T. Iitaka, and Y. Ma, Superconductive sodalite-like clathrate calcium hydride at high pressures, Proc. Natl Acad. Sci. USA **109**, 6463 (2012).

[25] H. Liu, I. I. Naumov, R. Hoffmann, N. W. Ashcroft, and R. J. Hemley, Potential high-Tc superconducting lanthanum and yttrium hydrides at high pressure, Proc. Natl Acad. Sci. USA **114**, 6990 (2017).

[26] A. G. Kvashnin, D. V. Semenok, I. A. Kruglov, I. A. Wrona, and A. R. Oganov, High-Temperature superconductivity in Th-H system at pressure conditions, ACS Appl. Mater. Interfaces **10**, 43809 (2018).

[27] F. Peng, Y. Sun, C. J. Pickard, R. J. Needs, Q. Wu, and Y. Ma, Hydrogen clathrate structures in rare earth hydrides at high pressures: Possible route to room-temperature superconductivity, Phys. Rev. Lett. **119**, 107001 (2017).

[28] I. Troyan, A. Gavriliuk, R. Rüffer, A. Chumakov, A. Mironovich, I. Lyubutin, D. Perekalin, P. Drozdov Alexander, and I. Eremets Mikhail, Observation of superconductivity in hydrogen sulfide from nuclear resonant scattering, Science **351**, 1303 (2016).

[29] V. S. Minkov, S. L. Bud'ko, F. F. Balakirev, V. B. Prakapenka, S. Chariton, R. J. Husband, H. P. Liermann, and M. I. Eremets, Magnetic field screening in hydrogen-rich high-temperature superconductors, Nat. Commun. **13**, 3194 (2022).

[30] V. S. Minkov, V. Ksenofontov, S. L. Bud'ko, E. F. Talantsev, and M. I. Eremets, Magnetic flux trapping in hydrogen-rich high-temperature superconductors, Nat. Phys. **19**, 1293 (2023).

[31] D. V. Semenok *et al.*, Effect of magnetic impurities on superconductivity in LaH_{10}, Adv. Mater. **34**, 2204038 (2022).

[32] I. A. Troyan *et al.*, Non-Fermi-liquid behavior of superconducting SnH_4, Adv. Sci. **10**, 2303622 (2023).

[33] See Supplemental Material at http://link.aps.org/supplemental/10.1103/PhysRevB.109.224515 for transport measurements; universal scaling of the *I-V* characteristics; pinning force in ThH_{10}; London penetration-depth estimations, which also includes Refs. [77,78].

[34] M. P. A. Fisher, Vortex-glass superconductivity: A possible new phase in bulk high-T_c oxides, Phys. Rev. Lett. **62**, 1415 (1989).

[35] G. Blatter, M. V. Feigel'man, V. B. Geshkenbein, A. I. Larkin, and V. M. Vinokur, Vortices in high-temperature superconductors, Rev. Mod. Phys. **66**, 1125 (1994).

[36] D. S. Fisher, M. P. A. Fisher, and D. A. Huse, Thermal fluctuations, quenched disorder, phase transitions, and transport in type-II superconductors, Phys. Rev. B **43**, 130 (1991).

[37] C. Dekker, W. Eidelloth, and R. H. Koch, Measurement of the exponent μ in the low-temperature phase of $YBa_2Cu_3O_{7-\delta}$ films in a magnetic field: Direct evidence for a vortex-glass phase, Phys. Rev. Lett. **68**, 3347 (1992).

[38] H.-h. Wen, H. A. Radovan, F. M. Kamm, P. Ziemann, S. L. Yan, L. Fang, and M. S. Si, 2D Vortex-glass transition with $T_g = 0$ K in $Tl_2Ba_2CaCu_2O_8$ thin films due to high magnetic fields, Phys. Rev. Lett. **80**, 3859 (1998).

[39] H. Yamasaki, K. Endo, S. Kosaka, M. Umeda, S. Yoshida, and K. Kajimura, Quasi-two-dimensional vortex-glass transition observed in epitaxial $Bi_2Sr_2Ca_2Cu_3O_x$ thin films, Phys. Rev. B **50**, 12959 (1994).

[40] Z. Sefrioui, D. Arias, M. Varela, J. E. Villegas, M. A. López de la Torre, C. León, G. D. Loos, and J. Santamaría, Crossover from a three-dimensional to purely two-dimensional vortex-glass transition in deoxygenated $YBa_2Cu_3O_{7-\delta}$ thin films, Phys. Rev. B **60**, 15423 (1999).

[41] W.-L. Zhao, X. Zhu, Z.-H. He, K.-H. Gao, and Z.-Q. Li, The vortex state in FeSe superconducting thin film, Supercond. Sci. Technol. **33**, 105010 (2020).

[42] H. Yang *et al.*, I−V characteristics of the vortex state in MgB_2 thin films, Phys. Rev. B **76**, 134513 (2007).

[43] C. Zhang, F. Hao, X. Liu, Y. Fan, T. Wang, Y. Yin, and X. Li, Quasi-two-dimensional vortex–glass transition and the critical

current density in TiO epitaxial thin films, Supercond. Sci. Technol. **31**, 015016 (2018).

[44] J. A. Fendrich, W. K. Kwok, J. Giapintzakis, C. J. van der Beek, V. M. Vinokur, S. Fleshler, U. Welp, H. K. Viswanathan, and G. W. Crabtree, Vortex liquid state in an electron irradiated untwinned YBa$_2$Cu$_3$O$_{(7-X)}$ crystal, Phys. Rev. Lett. **74**, 1210 (1995).

[45] A. Rydh, Ö. Rapp, and M. Andersson, Consistent description of the vortex glass resistivity in high-T_c superconductors, Phys. Rev. Lett. **83**, 1850 (1999).

[46] M. Andersson, A. Rydh, and Ö. Rapp, Scaling of the vortex-liquid resistivity in optimally doped and oxygen-deficient YBa$_2$Cu$_3$O$_{7-\delta}$ single crystals, Phys. Rev. B **63**, 184511 (2001).

[47] A. Yu *et al.*, Vortex glass phase transition in two-dimensional Bi$_2$Sr$_2$Ca$_2$Cu$_3$O$_{10+\delta}$ sub-microbridge, Supercond. Sci. Technol. **36**, 035008 (2023).

[48] M. Acosta, V. Sosa, and C. Acosta, Current-induced vortex glass transition in YBa$_2$Cu$_3$O$_x$ thin films, Superficies y Vacío **12**, 12 (2001).

[49] V. A. Vlasenko *et al.*, Evolution of vortex matter, phase diagram, and upper critical field in the FeSe$_{1-x}$S$_x$ system, Supercond. Sci. Technol. **34**, 035019 (2021).

[50] T. Klein, A. Conde-Gallardo, J. Marcus, C. Escribe-Filippini, P. Samuely, P. Szabó, and A. G. M. Jansen, Vortex-glass transition in the (K,Ba)BiO$_3$ cubic superconductor, Phys. Rev. B **58**, 12411 (1998).

[51] Y. Sun, J. Wang, W. Zhao, M. Tian, M. Singh, and M. H. W. Chan, Voltage-current properties of superconducting amorphous tungsten nanostrips, Sci. Rep. **3**, 2307 (2013).

[52] A. Y. Degtyarenko, I. Karateev, A. Ovcharov, V. Vlasenko, and K. Pervakov, Synthesis and HRTEM investigation of EuRbFe$_4$As$_4$ superconductor, Nanomaterials **12**, 3801 (2022).

[53] D. Dew-Hughes, Flux pinning mechanisms in type II superconductors, Philos. Mag.: A Theor. Exp. Applied. Phys. **30**, 293 (1974).

[54] T. T. M. Palstra, B. Batlogg, L. F. Schneemeyer, and J. V. Waszczak, Thermally activated dissipation in Bi$_{2.2}$Sr$_2$Ca$_{0.8}$Cu$_2$O$_{8+\delta}$, Phys. Rev. Lett. **61**, 1662 (1988).

[55] Y. Liu, T. Wang, Z. Xu, W. Hong, W. Peng, Z.-R. Lin, H. Luo, and G. Mu, Influences of quenching treatment and cobalt-doping on the thermally activated flux-flow behavior in KCa$_2$(Fe$_{1-x}$Co$_x$)$_4$As$_4$F$_2$, Supercond. Sci. Technol. **36**, 095008 (2023).

[56] A. V. Sadakov, V. A. Vlasenko, I. A. Troyan, O. A. Sobolevskiy, D. V. Semenok, D. Zhou, and V. M. Pudalov, Vortex phase dynamics in yttrium superhydride YH$_6$ at megabar pressures, J. Phys. Chem. Lett. **14**, 6666 (2023).

[57] Z. Liu, C. Wang, C. Xu, M. Hao, H.-M. Cheng, W. Ren, and N. Kang, Effects of domain structures on vortex state of two-dimensional superconducting Mo$_2$C crystals, 2D Mater. **6**, 021005 (2019).

[58] C. Zhang *et al.*, Observation of two-dimensional superconductivity in an ultrathin iron–arsenic superconductor, 2D Mater. **8**, 025024 (2021).

[59] S. Kumari, M. Anas, D. S. Raghav, S. Chauhan, P. K. Siwach, V. K. Malik, and H. K. Singh, A comparative study of superconductivity and thermally activated flux flow of YBa$_2$Cu$_3$O$_{7-\delta}$ and YBa$_2$Cu$_3$O$_{7-\delta}$/La$_{1-x-y}$Pr$_x$Ca$_y$MnO$_3$ bilayers, J. Supercond. Novel Magn. **35**, 3225 (2022).

[60] H. Zhang *et al.*, Anisotropic thermally activated flux-flow behavior in the layered superconductor 2M-WS$_2$, Phys. Rev. B **103**, L180503 (2021).

[61] Y. Eltsev, W. Holm, and Ö. Rapp, Transition from intact to short decoupled vortices in the vortex liquid of YBa$_2$Cu$_3$O$_{7-\delta}$, Phys. Rev. B **49**, 12333 (1994).

[62] S. Martin, A. T. Fiory, R. M. Fleming, G. P. Espinosa, and A. S. Cooper, Vortex-air excitation near the superconducting transition of Bi$_2$Sr$_2$CaCu$_2$O$_8$ crystals, Phys. Rev. Lett. **62**, 677 (1989).

[63] H. J. Jensen, P. Minnhagen, E. Sonin, and H. Weber, Vortex fluctuations, negative Hall effect, and thermally activated resistivity in layered and thin-film superconductors in an external magnetic field, Europhys. Lett. **20**, 463 (1992).

[64] M. V. Feigel'man, V. B. Geshkenbein, and A. I. Larkin, Pinning and creep in layered superconductors, Physica C **167**, 177 (1990).

[65] S. P. Obukhov and M. Rubinstein, Topological glass transition in entangled flux state, Phys. Rev. Lett. **65**, 1279 (1990).

[66] E. F. Talantsev and J. L. Tallon, Universal self-field critical current for thin-film superconductors, Nat. Commun. **6**, 7820 (2015).

[67] E. Talantsev, W. P. Crump, and J. L. Tallon, Thermodynamic parameters of single- or multi-band superconductors derived from self-field critical currents, Ann. Phys. **529**, 1700197 (2017).

[68] G. K. Perkins, L. F. Cohen, A. A. Zhukov, and A. D. Caplin, Implications of magnetic-hysteresis-loop scaling in high-temperature superconductors, Phys. Rev. B **51**, 8513 (1995).

[69] G. Prando, P. Carretta, R. De Renzi, S. Sanna, H. J. Grafe, S. Wurmehl, and B. Büchner, ac susceptibility investigation of vortex dynamics in nearly optimally doped RFeAsO$_{1-x}$F$_x$ superconductors (R = La, Ce, Sm), Phys. Rev. B **85**, 144522 (2012).

[70] M. J. Qin, X. L. Wang, S. Soltanian, A. H. Li, H. K. Liu, and S. X. Dou, Dependence of the flux-creep activation energy on current density and magnetic field for the MgB$_2$ superconductor, Phys. Rev. B **64**, 060505(R) (2001).

[71] L. Krusin-Elbaum, L. Civale, V. M. Vinokur, and F. Holtzberg, "Phase diagram" of the vortex-solid phase in Y-Ba-Cu-O crystals: A crossover from single-vortex (1D) to collective (3D) pinning regimes, Phys. Rev. Lett. **69**, 2280 (1992).

[72] J. Ge, J. Gutierrez, J. Li, J. Yuan, H.-B. Wang, K. Yamaura, E. Takayama-Muromachi, and V. V. Moshchalkov, Dependence of the flux-creep activation energy on current density and magnetic field for a Ca$_{10}$(Pt$_3$As$_8$)[(Fe$_{1-x}$Pt$_x$)$_2$As$_2$]$_5$ single crystal, Appl. Phys. Lett. **104**, 112603 (2014).

[73] Y. Yeshurun and A. P. Malozemoff, Giant flux creep and irreversibility in an Y-Ba-Cu-O crystal: An alternative to the superconducting-glass model, Phys. Rev. Lett. **60**, 2202 (1988).

[74] M. Tinkham, Resistive transition of high-temperature superconductors, Phys. Rev. Lett. **61**, 1658 (1988).

[75] H.-S. Lee, M. Bartkowiak, J. S. Kim, and H.-J. Lee, Magnetic-field-induced crossover of vortex-line coupling in SmFeAsO$_{0.85}$ single crystal, Phys. Rev. B **82**, 104523 (2010).

[76] J. Kim, F. Ronning, N. Haberkorn, L. Civale, E. Nazaretski, N. Ni, R. J. Cava, J. D. Thompson, and R. Movshovich, Large

magnetic penetration depth and thermal fluctuations in a superconducting $Ca_{10}(Pt_3As_8)[(Fe_{1-x}Pt_x)_2As_2]_5$ ($x = 0.097$) single crystal, Phys. Rev. B **85**, 180504(R) (2012).

[77] J. E. Hirsch and F. Marsiglio, On magnetic field screening and trapping in hydrogen-rich high-temperature superconductors: Unpulling the wool over readers' eyes, J. Supercond. Novel Magn. **36**, 1813 (2023).

[78] V. S. Minkov, S. L. Bud'ko, F. F. Balakirev, V. B. Prakapenka, S. Chariton, R. J. Husband, H. P. Liermann, and M. I. Eremets, Author correction: Magnetic field screening in hydrogen-rich high-temperature superconductors, Nat. Commun. **14**, 5322 (2023).

[79] https://github.com/mark6871/ThH10-and-ThH9/tree/ThH10-R(T%2CH).